

# Registering External and Internal Morphological Images of Coronary Vessels

P Radeva, D Rotger, E Nofrerias and J Mauri<sup>†</sup>  
Computer Vision Center, University Autònoma of Barcelona  
<sup>†</sup> University Hospital Germans Trias i Pujol

## Abstract

The growing appreciation of the pathophysiological and prognostic importance of arterial morphology has led to the realization that angiograms are inherently limited in defining the distribution and extension of coronary wall disease. By Intravascular Ultrasound images physicians have a picture of the composition of vessel in detail. However, observing an intravascular ultrasound stack of images, it is difficult to figure out the image position and extension with regard to the vessel parts and ramifications, and misclassification or misdiagnosis of lesions is possible. The objective of this work is to develop a computer vision technique to fuse the information from angiograms and intravascular ultrasound images defining the correspondence of every ultrasound image with a corresponding point of the vessel in the angiograms.

## KEY WORDS:

coronary vessels, lesion detection, angiograms, IVUS, multimodal image fusion, deformable models

## 1 Introduction

According to the American Heart Association coronary heart disease (CHD) caused 459,841 deaths in the United States in 1998 (1 of every 5 deaths) [1]. This figure is easy to extrapolate to the most of the developed countries along the western world.

IntraVascular UltraSound (IVUS) images have allowed deepening in the knowledge of the true extension of the coronary vessel illness [2, 3, 4, 5]. It is a tomographic image that provides a unique 2D *in vivo* vision of the internal vessel walls (figure 1(a)), determining the extension, distribution and treatment of the atherosclerotic, fibrotic plaques and thrombus, and their possible repercussion on the internal arterial lumen. Angiography images provide an external vision of the vessel shape and tortuosity (figure 1(b)). The main difference between the ultrasound and the angiography images, as the most used image modalities for vessel diagnosis, deals with the fact that the most of the visible plaque lesions with IVUS are not evident with angiogram.

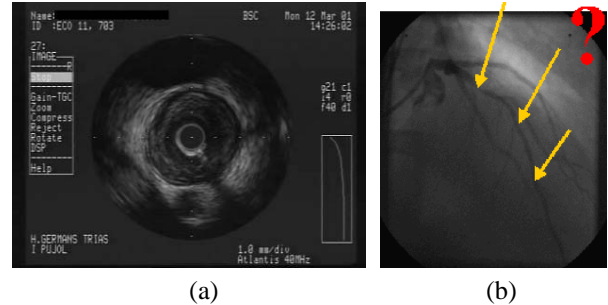


Figure 1. (a) IVUS image. (b) Corresponding angiography.

Studies on intravascular ecography have shown that the reference vessel segment has the 35-40% of its sectional area occluded because of the plaque, although it appears as normal in the angiography. Besides its capacity of demonstrating the plaque extension and distribution inside the vessels, IVUS offer information about the composition of the internal lesion; in particular, about calcium deposits as the most important isolated predictors to evaluate if a particular lesion will respond to a catheter treatment.

The studies about stents<sup>1</sup> carried out with IVUS show that the appearance in the angiography of a good stent deployment can hide two possible problems: the incomplete apposition (a portion of the stent is not making pressure on the vessel wall) and the incomplete expansion (a portion of the stent remains closed although the expansion of the rest of the stent areas). Both problems are very significant since they can be worse than the problem they are trying to solve.

Both methods (IVUS and angiogram) provide a lot of information about the internal and the external shape of the coronary vessels, respectively, as well as about vessel therapy (e.g. stent, etc.). The fusion of all this information will allow the physicians to interact with the real extension and distribution of the disease in the space, making easier the arduous task of having to imagine it.

One of the problems of dealing with IVUS is the fact that the images represent a 2D plane perpendicular to the catheter without any depth information. This IVUS property hides the real disease's extension and represents a very unnatural way of conceptualization. The foremost limita-

<sup>1</sup>Spiral metallic mesh implanted inside a coronary vessel to save the stenosis effect



Figure 2. Siemens C-Arm angiocardiographic system.

tion of IVUS on the pre- and post-treatment studies is the need of correlating lesion images in serial studies. This limitation is due to the lack of third dimension that gives much more global information about the internal and external vessel structure. This problem can be solved by using the information given by the angiographies. Using two projections in fixed angles and taking into account the calibration parameters, we are able to create a curve in the space representing the catheter tortuosity. It allows to place IVUS images and define exact correspondence between data coming from both image modalities.

The article is organized as follows: section 2 is devoted to the 3D reconstruction of the catheter from multiple views of angiograms. Section 3 discusses the process of locating IVUS images in space. Section 4 explains the validation process and the article finishes with conclusions.

## 2 3D Reconstruction of IVUS Catheter from Angiograms

Intravascular ultrasound images are acquired during a pull-back of catheter through the vessel. Using an angiogram-guided process, the catheter is introduced in the vessel to diagnose, and positioned after the vessel lesion. Afterwards, a pullback with constant speed is performed acquiring the IVUS images. Therefore, the obtained stack/sequence of images define a spatio-temporal data that allow to scan the morphology of the vessel lesion in space.

In order to locate IVUS images in space we need an 3D reconstruction of the catheter trajectory. To this purpose, we need to register the catheter in two views of angiograms before and after the pullback of the IVUS catheter. Moreover, to assure precise 3D reconstruction of the catheter from both X-ray views, minimal spatial displacement of the catheter should occur during the process of acquisition of multiple views of X-ray images. A bi-plane X-ray system provides two views of the catheter at the same time that yield better conditions for a precise 3D reconstruction of the catheter. However, today many hos-

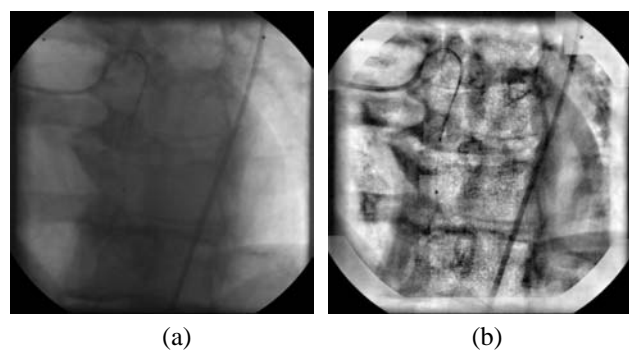


Figure 3. (a) Original X-ray image and (b) after applying local enhancement.

pital environments are equipped with mono-plane X-ray devices (figure 2). Considering the general case, given a mono-plane X-ray image system, we use ECG-gated X-ray images and the patient is asked to keep its breathing during an instant X-ray image acquisition in order to keep minimal spatial displacement of the catheter.

At this stage, our aim is to create a model of the catheter recovering its tortuosity in the space from its projections in both X-ray images. Given that X-ray images are characterized with low signal-to-noise rate, an image enhancement step is necessary in order to improve the visualization and the performance of the following processing algorithms. We perform a histogram-based local image enhancement (see fig. 3) of X-ray images defined as follows:

$$I(x, y) = (I(x, y) - a)/(b - a),$$

$$a = \min_{x' \in N, y' \in N} I(x', y')$$

$$b = \max_{x' \in N, y' \in N} I(x', y')$$

where  $N(x, y)$  is a neighborhood of pixel  $(x, y)$  of fixed size.

At this stage, the physician is asked to locate the end of the catheter before and after the pullback in both views of angiograms and two 3D points are reconstructed. Note that these points represent the center of first and last IVUS images (see fig.4). A short review of the spatial reconstruction process of an 3D point from its projections is given in the Appendix. For more details, one can consult the reference [6].

The reconstruction of the whole trajectory of the catheter contains 2 steps: a) detection of the catheter projection from both views, and b) reconstruction of its trajectory in space. The process of catheter projection consists of applying the fast marching algorithm that allows to find a path with minimal geodesic distance between two points of an image [7]. The fast marching algorithm is a segmentation algorithm that is based on the level set theory. A surface of minimal action (SMA) is constructed as a level set of curves  $L$  where the level corresponds to the geodesic distance  $C\{L\}$  from an initial point  $A$ . Thus, each point,  $p$  from the SMA,  $U$  has a value  $U(p)$  equal to the integral

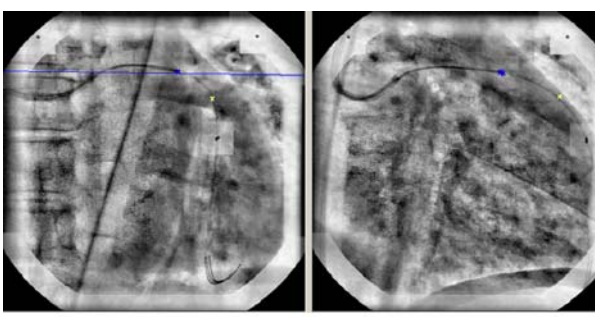


Figure 4. Localization of catheter head before and after IVUS pullback.

minimal energy of the geodesic path  $P$  starting from the initial point  $A$  and ending at point  $p$ :

$$U(p) = \inf_{C\{L\}=p} \int \tilde{P} ds$$

It can be shown that the path of minimal geodesic distance from point  $B$  to  $A$  can be constructed by following the normal direction of the level sets beginning from this passing through point  $B$  (see fig. 5).

Once both projections of the catheter has been obtained,  $M$  equidistant points from one of the projections are chosen. It is easy to show that their corresponding points are the intersections of the corresponding epipolar lines and the detected catheter projection in the other X-ray view (see fig. 6). Once defined the corresponding points from both angiograms, their 3D points are reconstructed and interpolated by a spatial B-spline curve [8] that represents the 3D reconstruction of the catheter path done between the beginning and the end of the pullback (see fig. 5). Note that this spatial curve represents the trace of the centers of the IVUS images.

As a result, considering two projections with the catheter stopped before the pullback begins and another two at the end, we create a curve model of the pullback situating one model's extreme at the position of the IVUS catheter before the pullback begins and, using the projections taken at the end of the pullback, situate the ending extreme of the model coinciding with the last position of the catheter during its pullback.

### 3 Locating IVUS Images on the 3D Catheter Model

Our next goal is to place each IVUS plane in space in order to allow later reconstruction of vessel tortuosity. The position of each IVUS image is determined by IVUS catheter trajectory. Most IVUS acquisition systems grab and save image sequence in an S-VHS videotape, some of them assuring constant speed of the catheter movement (0.5mm/sec or 1mm/sec). To analyse IVUS information and fuse it with angiograms, a digitalization of IVUS im-

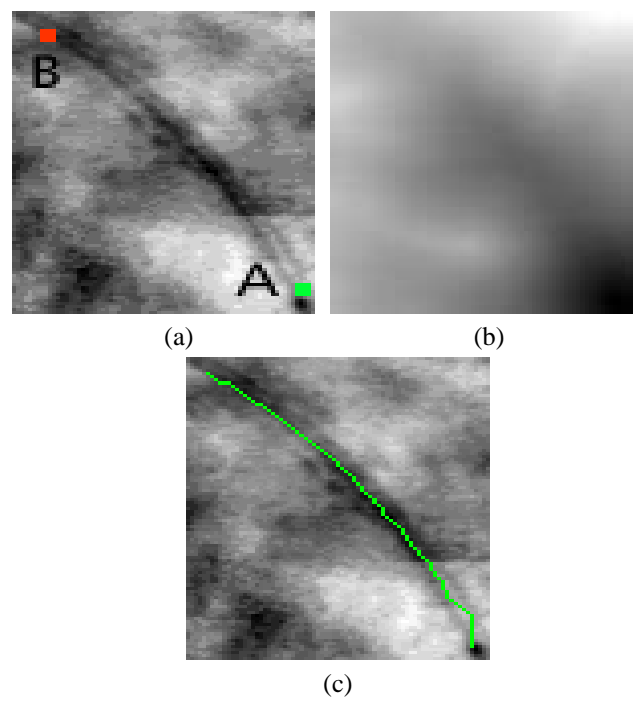


Figure 5. (a) Preprocessed X-ray image, (b) surface of minimal action and (c) geodesic path between points A and B.

ages is necessary (we used a frame grabber to digitize images at 25 frames per second).

The task of registering IVUS data with angiogram information transforms to situating the IVUS images along the 3D curve. Although using an automatic catheter pullback of constant speed (0.5mm/s), we detected different phases of the catheter movement once the pullback has been switched on: Delay Before pullback (DB), Positive Acceleration phase (PA), phase of Constant Movement (CM) of the catheter and Negative Acceleration phase (NA). Taking into account these characteristics of the catheter movement and the backprojection of the 3D catheter trajectory, we can precisely determine the exact correspondence of IVUS data with the vessel from the angiograms.

We start positioning the last IVUS image at the curve's extreme, corresponding to the ending of the pullback, perpendicular to the curve and go on situating the other images along the curve at a distance given by the pullback speed and the images discretization. To this purpose, we have to calculate the normals and binormals of the 3D curve. Given that we are using B-Splines, we can analytically calculate the Frenet triangle  $(\vec{t}, \vec{n}, \vec{b})$ , where  $\vec{t}$  is the curve tangent,  $\vec{n}$  is the curve normal and  $\vec{b}$  is the curve binormal of the B-spline catheter model. We take into account that the IVUS image plane is perpendicular to the catheter that means that coincides with the normal plane defined by the normal and binormal of the catheter model. Thus, taking into account the distance the catheter head has moved from the end point of the catheter model (computed

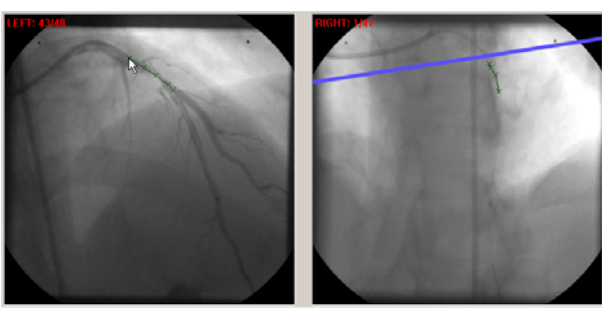


Figure 6. Each point on the catheter projection defines its corresponding point by the epipolar line on the other X-ray view.

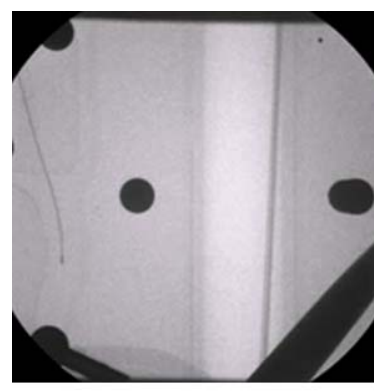


Figure 8. Phantom used to estimate catheter movement.

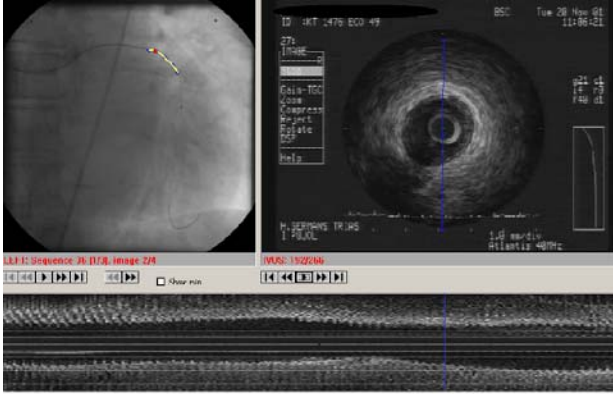


Figure 7. Registration of angiogram and IVUS data: the red point in the angiogram (top on the left) corresponds to IVUS transversal plane (top on the right) and to the blue line in the longitudinal view of IVUS data (bottom)

from IVUS data) and the 3D length of the catheter model (computed from the angiograms data), we can locate the IVUS plane in space.

It can be shown that using the triangle of Frenet creates an artificial rotational effect of IVUS planes around the tangent direction of the catheter. In order to minimize the rotational transformation between two consecutive planes, we project the normal and binormal vectors of the previous IVUS plane to the actual one, applying the following formulae:

$$\vec{n}_i = \vec{n}_{i-1} - \vec{t}_i * (\vec{n}_{i-1} \cdot \vec{t}_{i-1})$$

$$\vec{b}_i = \vec{t}_i \times \vec{n}_i$$

Once placed all IVUS images along the 3D curve of the catheter model that is described during the catheter pullback, we can determine the correspondence between IVUS and angiogram data (see fig.7). This fact allows to the user to define corresponding data between angiograms and IVUS data. Note that this fact is very important since angiograms give information about the external view of the vessels, distance to ramifications, lesions, stents and other

anatomic parts of the hearts, while IVUS images provide information about the internal shape of the vessel e.g. its morphological structure, vessel wall thickness and composition, plaque, calcium deposits, etc.

## 4 Results and Validation

Given that the different cycles of the catheter motion depend on the catheter mechanical properties, we estimated them on a phantom provided by Boston Sci (see fig.8). We performed 13 pullback image acquisition on a phantom and estimated the mean and standard deviation of measurements. The mean velocity of the catheter is shown in fig.9 and the estimates of the different phases are given in table 1.

Coupling both information from multimodal images permits to know where IVUS images are in space as well as to show the IVUS image corresponding to given point of the angiography. The user has to select a point on the angiography. Then, automatically its corresponding point on the other X-ray image is determined using the epipolar line. Doing a back-propagation of the given point, the 3D point is reconstructed in the space. From the position of the desired point on the 3D model of the pullback, the nearest IVUS image to the point is determined. Moreover, its position in the longitudinal IVUS images is visualized. Analogously, given a short-axis IVUS image, its position in the IVUS stack is visualized in the longitudinal IVUS data and the corresponding 3D point and its projection on the X-ray image is displayed to the physician (see fig.7).

In order to validate the proposed approach we proceeded with two groups of tests: *in-vivo* and *in-vitro*. The first group of tests had as a purpose to validate the approach avoiding the artifacts coming from the vessel motion. We used 7 IVUS pullbacks on a phantom (see fig. 10) provided by Boston Scientific with a calcium deposit (CD). Once reconstructed the catheter path in space and detected the CD on the IVUS image, we estimated its position in space and tested its appearance from the angiograms. Note

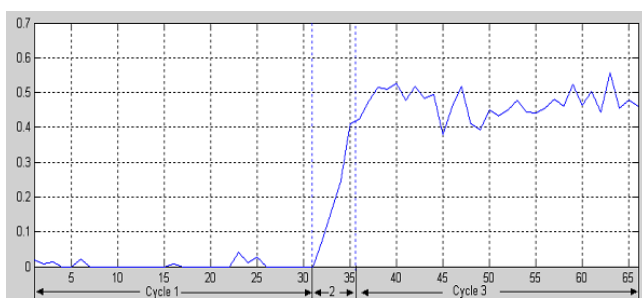


Figure 9. Average movement speed of the catheter measured on a phantom.

Phase	mean	std.
<i>DB</i>	5.2353s (2.6177mm)	0.2712s (0.1356mm)
<i>PA</i>	0.2749s (0.1375mm)	0.1942s (0.0971mm)
<i>CM</i>	0.9934s (0.4967mm)	0.2031s (0.1015mm)
<i>NA</i>	0.0218s (0, 0109mm)	0.6243(0.3121mm)

Table 1. Mean and std of different phases of catheter movement.

that the second IVUS images in fig. 10 corresponds to a point in the X-ray image before the calcium deposit, while the third IVUS image visualizing calcium corresponds to a point in the X-ray image inside the deposit. The mean error of CD estimate was  $0.3mm$  with standard deviation  $\sigma = 0.42mm$ . We explain the localization error by the human voice annotation of the pullback start and end as well as the impossibility of recording images with precision higher than a second in the current IVUS acquisition systems.

We have also tested the system with 3 real cases of patients in the Hospital Universitari "Germans Trias i Pujol" of Badalona. Patients with vessels lesion that contain calcium deposits have been chosen and again the procedure of validating the registration between angiograms and IVUS images was performed. The results showed a mean error of  $\mu_{error} = 1.027mm$  with standard deviation of  $\sigma_{error} = 1.2154mm$ . The localization error increases due to the vessel motion that leads to less precise 3D reconstruction of the catheter trajectory. Nevertheless, this error is confirmed by the physician team as acceptable to the purposes of lesion localization.

## 5 Conclusions

Fusing IVUS and angiogram data is of high clinical interest to help the physicians locate in IVUS data and decide which lesion is observed, how long it is, how far from a bifurcation or another lesions stays, etc. In this study, we developed tools to estimate and show the correspondence

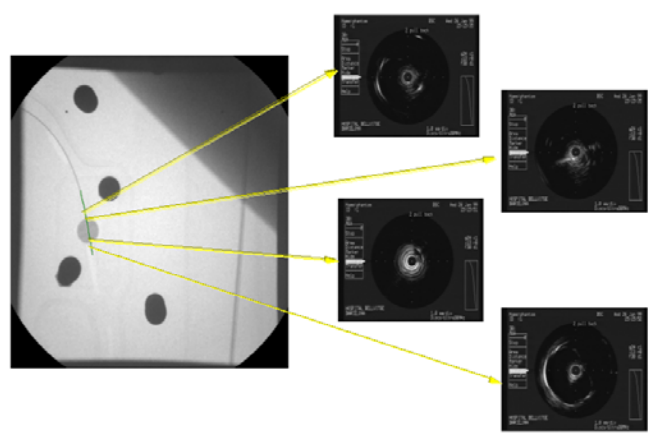


Figure 10. Validation of localizing calcium deposit by a phantom.

between IVUS images and vessels in angiograms and have validated it on an IVUS phantom and patient data.

## References

- [1] Association AH. 2001 heart and stroke statistical update. 2000;Dallas, Texas: American Heart Association, <http://www.americanheart.org/>.
- [2] Kearney P, Starkey I, Sutherland G. Intracoronary ultrasound: Current state of the art. British Heart Journal Supplement 2 1995;73:16–25.
- [3] Zhang X, McKay C, Sonka M. Image segmentation and tissue characterization in intravascular ultrasound. IEEE Medical Imaging 1998;17:880–899.
- [4] Sonka M, Zhang X, Siebes M, Bissing M. Segmentation of intravascular ultrasound images: A knowledge-based approach. IEEE Transactions on Medical Imaging 1995;14:719–732.
- [5] Birgelen CV, Slager C, Mario CD, de Feyter P, Seruys W. Volumetric intracoronary ultrasound a new maximum progression-regression of atherosclerosis. Atherosclerosis 118 Suppl 1995;.
- [6] A.C.M. Dumay J.H.C. Reiber JG. Determination of optimal angiographic viewing angles: Basis principles and evaluation study. IEEE Medical Imaging 1994; 13:13–23.
- [7] Cohen LD, Kimmel R. Global minimum for active contour models: A minimal path approach. International Journal of Computer Vision August 1997; 24(1):57–78.
- [8] B.A.Barsky R.H.Bartels J. An Introduction to Splines for use in Computer Graphics and Geometry Modeling. Morgan Kaufmann Publishers INC, 1987.

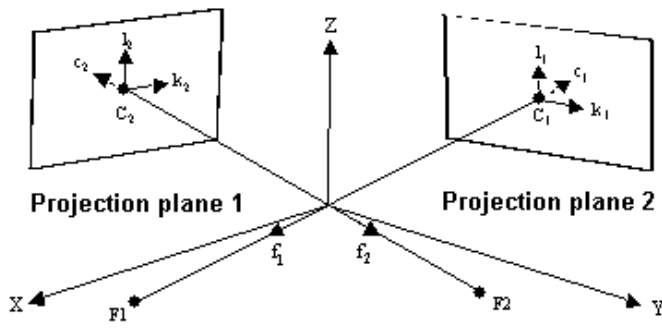


Figure 11. Global reference system (x,y,z) with the projection planes and their local systems.

## Appendix

The projection axes of both systems intersect in the *isocenter* [6]. The acquisition parameters (distances from the X-Ray sources to the image intensifiers, angles of rotation and angulation) are predetermined before the image acquisition process.

The angles by which a left-right movement of a system, with respect to the patient, can be defined determine the rotational angles. The angles by which a movement of a system can be defined towards the head of the patient (Cranial (CR) direction) or the feet (Caudal (CA) direction) determine the angulation angles. With the imaging equipment, the heart can be displayed under X-Ray exposure from Left Anterior Oblique (LAO) view to a Right Anterior Oblique (RAO) view, with either a cranial or caudal angulation. Rotational angles are denoted by  $\alpha$  and angulation angles by  $\beta$ . For the frontal and lateral rotation angles  $\alpha > 0$  represent LAO views,  $\alpha < 0$  represent RAO views; angulation angles  $\beta > 0$  represent caudal views and  $\beta < 0$  represent cranial views.

For a three-dimensional reconstruction of the catheter, we define a global reference system with origin in the isocenter. We also define a local reference system on the image plane to allow the conversion from an image point to the global reference system (figure 11).

The equations to calculate the local reference system are:

$$\begin{aligned}\vec{k} &= (0, -\cos \alpha, \sin \alpha)^T \\ \vec{c} &= (\sin \beta, \sin \alpha \cos \beta, \cos \alpha \cos \beta)^T \\ \vec{l} &= \vec{k} \times \vec{c}\end{aligned}$$

A data point in the image matrix with coordinate pair  $(x, y)$  is transformed into a pair of real coordinates  $(x_k, y_k)$  in the projection plane by:

$$x_k = c_{cal}x \text{ and } y_l = c'_{cal}y$$

Here,  $c_{cal}$  is the calibration factor and  $c'_{cal}$  is the calibration factor corrected for the pixel aspect ratio. We are

now able to identify a given point in one image plane in the other image by projecting the epipolar line corresponding to that point in the other projection plane. The epipolar line in the second projection plane of a point  $d_1$  in the first projection plane is computed from:

$$\nu \vec{f}_1 \vec{f}_2 + \mu \vec{f}_1 \vec{d}_1 + \vec{F}_1 = x_k \vec{k}_2 + y_l \vec{l}_2 + \vec{C}_2$$

The line  $y_l(x_k)$  is represented in the image matrix as  $y(x)$  by applying the inverse transform of (1).

The spatial location of a 3D point can be computed from both projections of this point (back-projection). The spatial position of this point is computed by a simple intersection of the lines with vector representation:

$$\vec{F}_1 + \tau \vec{f}_1 \vec{d}_1 \text{ and } \vec{F}_2 + \sigma \vec{f}_2 \vec{d}_2$$

Both parameters  $\tau$  and  $\sigma$  are solved from any two of the three equations of the vector components by elimination of the other parameter [6].